A Model and Observations of Time-Dependent Upwelling over the Mid-Shelf and Slope[1]

G. S. JANOWITZ AND L. J. PIETRAFESA

Department of Marine Science and Engineering, North Carolina State University, Raleigh 27650

(Manuscript received 28 January 1980, in final form 17 July 1980)

ABSTRACT

A simple model of time-dependent quasi-geostrophic upwelling over an outer continental shelf and slope region is considered with the velocity assumed independent of the alongshore coordinate. The flow is at rest and stably stratified when a uniform alongshore wind stress τ is applied. Initially, the onshore flow in the water column balances the offshore top Ekman volume flux. As time progresses the bottom Ekman layer supplies increasingly more of the required onshore flux and the onshore flow in the interior of the water column decreases. The shallower water spins up first leading to both a coastal jet and an upward bulge in the isopycnal surfaces which propagates offshore with a speed equal to $0.012(\tau/\rho)^{1/2}/h_x$, where h_x is the local slope. At the shelf break, if $h_{xx}h/h_x^2 > 2$ another upward bulge of the isopycnal surfaces will develop at the onset of upwelling favorable winds and will be of greater amplitude than the propagating bulge. The theory is generalized to include the effects of a time-dependent wind stress and those of a specified time-dependent alongshore pressure gradient. The velocity induced by the deformation of the density field is then calculated. Comparisons of theory with moored meter data collected in Onslow Bay, North Carolina are made during upwelling favorable summertime wind conditions.

1. Introduction

The literature on wind-induced coastal upwelling, from both the theoretical and observational points of view (cf. O'Brien, 1975; Csanady, 1977; Allen, 1980), has expanded considerably in the past decade. Recently, much of the theoretical efforts have been directed at the important region of active upwelling in the near coastal region where horizontal mixing and baroclinic effects are of prime importance. This region has also been addressed observationally during recent continental shelf studies conducted off Oregon, West Africa, Peru and North Carolina. It has been found that this coastal boundary zone exists primarily to close the circulation pattern, i.e., to inject mass into the upper Ekman layer, to bring the alongshore velocity to rest, and is at most a few tens of kilometers wide. Over wide shelves the effects of baroclinicity and horizontal mixing may not be of prime importance outside of the coastal boundary layer and it is the flow in this outer region that the present work addresses. The relatively few models which may apply to this region either treat the physics as being steady (e.g., Garvine, 1971; Hsueh and Ou, 1975; Lill, 1979) or as that of forced shelf waves (Allen, 1980). The observed circulatory response on the North Carolina shelf to wind forcing is neither steady (Blanton and Pietrafesa, 1978) nor influenced by either free or forced southerly propagating continental shelf waves (Pietrafesa and Janowitz, 1980). As borne out in coastal sea level and moored current meter data (Pietrafesa, 1979), long waves are being advected to the north with the Gulf Stream in this region of the South Atlantic Bight and the cross-shelf influence of these waves can be considerable on the outer 10–40 km of the shelf. The zone between the inner shelf and shelf break, however, is principally wind dominated. It is the flow in this region, during upwelling favorable wind conditions, that we examine from theoretical and observational perspectives in this paper.

In Section 2 we formulate a simple model in which the stratification is sufficiently weak so that the density may be treated as a passive scalar. In Section 3 the results from this model are obtained and discussed, the magnitude of the friction parameters are discussed, and the model is generalized to encompass the effects of time-dependent winds and alongshore pressure gradients. In Section 4, the magnitude of the terms hitherto neglected are calculated and the range of validity of the solution is determined. The small correction due to the previously calculated density disturbance is also obtained in this section. Finally, in Section 5, a comparison of predictions and observations of the flow in Onslow Bay, North Carolina, is undertaken.

[1] Contribution No. 80-3 from MSE-NCSU.

0022-3670/80/101574-10$06.50

2. Formulation

We consider a shelf-slope region with a depth $h(x)$ which increases monotonically with the offshore coordinate x, and is independent of the alongshore coordinate (see Fig. 1). The Coriolis parameter f is assumed constant. Initially a vertically stratified $[\rho = \rho_0(z)]$ fluid is at rest over this region. At $t = 0$, a uniform alongshore wind stress of magnitude τ is applied in the positive along-shore direction. We seek a solution independent of the alongshore coordinate for the quasi-geostrophic motion induced by the wind stress under the rigid lid, Boussinesq and hydrostatic approximations. Additionally, we assume that the top and bottom boundary layers are thin compared to the depth and that the effects of nonlinear and horizontal mixing terms are of secondary importance. The dependent variables are decomposed into an interior solution which exists for all x, z, t, and top and bottom boundary-layer corrections which decay away from their respective boundaries. When the alongshore momentum equation is integrated in the vertical under the above assumptions and the constraint that the net onshore flux is zero, we obtain

$$\int_{-h}^{0} v_t dz = (\tau - \tau_B)/\rho_r. \tag{1}$$

The alongshore flux associated with the boundary layers can be shown to be small compared with that associated with the interior solution alongshore velocity given in (1). We shall examine the flow under two alternative parameterizations of the bottom stress τ_B. We consider both linear and nonlinear relations for this quantity and shall define a length scale associated with each parameterization.

For the linear bottom stress relation we take

$$\tau_B = \rho_r c_1 v(x, -h, t), \tag{2a}$$

$$d \equiv c_1/f. \tag{2b}$$

For the nonlinear parameterization we take

$$\tau_B = \rho_r c_2 |v| v(x, -h, t), \tag{3a}$$

$$d \equiv (\tau c_2/\rho_r f^2)^{1/2}. \tag{3b}$$

We note that if the bottom layer where taken to have a constant eddy diffusivity A_v, then $d = (A_v/2f)^{1/2}$ which is approximately one-sixth of the standard Ekman-layer depth.

The equations which govern the interior velocity field u, v and w, and the density and pressure disturbances due to the wind-induced motions under the previously stated assumptions are as follows:

$$v = p_x/\rho_r f, \tag{4a}$$

$$u = -v_t/f, \tag{4b}$$

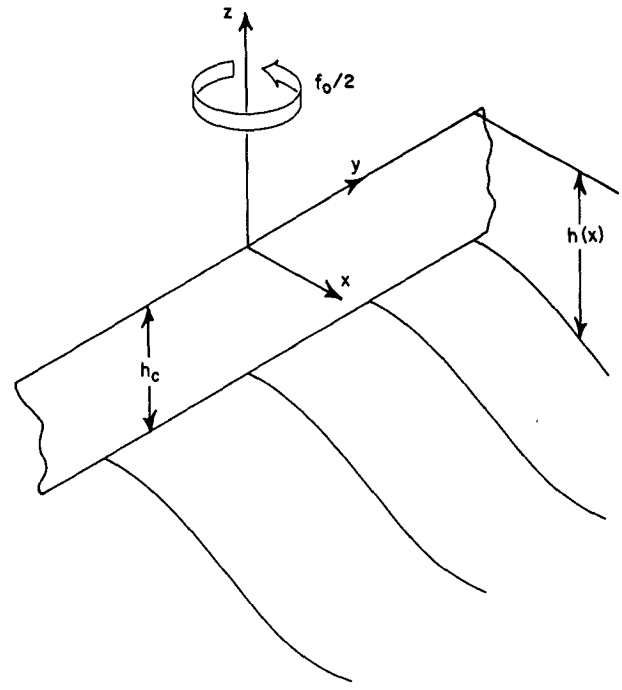

FIG. 1. Geometry of the region.

$$p_z = -\rho g, \tag{4c}$$

$$u_x + w_z = 0, \tag{4d}$$

$$\rho_t = -\rho_{0z}(z) w. \tag{4e}$$

We can show *a posteriori* that the ratio of the baroclinic to barotropic horizontal velocities is of order $g|\rho_{0z}|h_x^2/f^2$ which we now take to be small compared to 1. The horizontal velocity will be taken to be independent of depth and the density will be treated as a dynamically passive scalar. In Section 4, baroclinic effects will be calculated for a linearly stratified fluid. We now proceed to a calculation of the wind-stress-induced motion.

3. Solution and discussion

Eqs. (1) and (4) can be written, with the use of (2) or (3), as

$$hv_t + \begin{Bmatrix} c_1 v \\ c_2 v|v| \end{Bmatrix} = \tau/\rho_r, \tag{5a}$$

$$u = -v_t/f, \tag{5b}$$

$$w = -zu_x = zv_{xt}/f, \tag{5c}$$

$$\rho_t = -\rho_{0z}(z) w = -z\rho_{0z}(z) v_{xt}/f$$

or

$$\rho = -z\rho_{0z}(z) v_x/f. \tag{5d}$$

In Eq. (5a), the upper (lower) term in the braces is used if the linear (nonlinear) bottom stress relation is utilized. Eq. (5a) can readily be integrated under

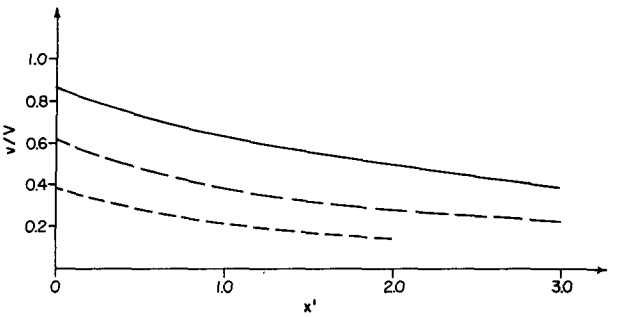

FIG. 2. Alongshore velocity versus offshore distance for $\eta_c = 0.500$ (– – –), $\eta_c = 1.00$ (— —), $\eta_c = 2.00$ (——) for the linear bottom stress case.

the initial condition that $v(x,0) = 0$. It is convenient to define an alongshore velocity scale V and a dimensionless spin-up time η as

$$V \equiv \tau/\rho_r fd, \tag{6a}$$

$$\eta \equiv fdt/h. \tag{6b}$$

The solution for the linear bottom-stress relation is

$$v = V(1 - e^{-\eta}), \tag{7a}$$

$$u = -(Vd/h)e^{-\eta}, \tag{7b}$$

$$w = (Vd|z|/h^2)h_x(1 - \eta)e^{-\eta}, \tag{7c}$$

$$\rho = |z\rho_{0z}(z)|(Vh_x/fh)\eta e^{-\eta}, \tag{7d}$$

$$\rho_x = -|z\rho_{0z}(z)|(Vh_x^2/fh^2) \times (2 - \eta - h_{xx}h/h_x^2)\eta e^{-\eta}. \tag{7e}$$

For a time-dependent alongshore wind stress $\tau(t)$, Eq. (5a) can be integrated for the linear bottom stress relation and we obtain

$$\rho_r hv = \int_0^t \tau(t') \exp[-fd(t - t')/h]dt'. \tag{8}$$

The remaining variables u, w and ρ can be obtained from Eqs. (5b)–(5d) for a time-dependent wind when Eq. (8) is used.

If, in addition to a time varying wind stress, a time varying alongshore pressure gradient independent of x, y and z were imposed on the system, the term $-hp_y(t)/\rho_r[-p_y(t)/\rho_r f]$ should be added to the right-hand side of (5a) [(5b)]. Eq. (8) would then have $\tau(t')$ augmented by $-hp_y(t')$. The effects of an alongshore pressure gradient are explored more fully in the Appendix.

For the nonlinear bottom stress relation, we can obtain the solutions

$$v = V \tanh\eta, \tag{9a}$$

$$u = -(dV/h) \operatorname{sech}^2\eta, \tag{9b}$$

$$w = (dV|z|/h^2)h_x(1 - 2\eta \tanh\eta) \operatorname{sech}^2\eta, \tag{9c}$$

$$\rho = |z\rho_{0z}(z)|(Vh_x/fh)\eta \operatorname{sech}^2\eta, \tag{9d}$$

$$\rho_x = -|z\rho_{0z}(z)|(Vh_x^2/fh^2) \times (2 - h_{xx}h/h_x^2 - 2\eta \tanh\eta)\eta \operatorname{sech}^2\eta. \tag{9e}$$

No generalization for a time-dependent wind stress can be obtained for the nonlinear bottom-stress case. The scales of the variables are the same for linear and nonlinear bottom stress laws and the spin-up process is quite similar in both cases with the process occurring more rapidly for the nonlinear relation. Therefore, in discussing the solution we shall only discuss the case of the linear bottom-stress relation.

With the onset of the upwelling favorable wind an offshore volume flux $\tau/\rho_r f$ is set up in the top Ekman layer. An onshore interior flow is set up to replace the offshore transport. As the depth increases the onshore velocity must decrease in magnitude, as $u|_{t=0} = -\tau/\rho_r fh$. The Coriolis force due to the on-shore flow sets up an alongshore current and the bottom boundary layer associated with this current. The bottom layer carries mass toward the coast which allows the onshore flow to decrease in magnitude. Since the on-shore flow and its associated Coriolis force is a maximum in shallow water, the alongshore velocity is a maximum there, and the vorticity associated with this current (v_x) is negative. In Fig. 2, we plot v/V versus x for three different times. We take $h = h_c + \alpha x$ and $x' \equiv \alpha x/h_c$; the three times are chosen so that at $x = 0, fdt/h_c = 0.5, 1.0, 2.0$.

Early in the upwelling process, when $\eta < 1$ for all x, the vertical velocity is positive everywhere reflecting the kinematic effect ($w_B = -uh_x$). When $\eta_c > 1$ the vertical velocity is negative at the coast. This occurs because the downward suction into the bottom layer ($v_x < 0$) overcomes the weakening kinematic effect. As time increases still more, the vertical velocity will be negative in ever wider regions of shallow water while still positive in deep water. This somewhat unusual result follows from the role played by the bottom layer.

The density disturbance is simply the time integral of the vertical velocity. It is positive for all time and reaches a maximum when $\eta = 1$. In Fig. 3 we plot

$$\rho' \equiv \rho/[|z\rho_{0z}(z)|(Vh_x/fh)]$$

versus η; at a fixed location this is a plot of the time history of the density disturbance.

The shape of the isopycnal surfaces at a fixed time reflects the variation of ρ with h, η and h_x. We first consider a topography with h_x = constant. From Eq. (7e), we see that for early times, when $\eta < 2$ everywhere, $\rho_x < 0$. The isopycnal surfaces slope upward as we move into shallow waters. For $\eta_c > 2$, the isopycnal surfaces slope upward (downward) in the onshore direction in deep (shallow) water as $\rho_x < 0$ (>0) there. This implies that an upward bulge in these surfaces exists with the crest at

$h = fdt/2$ ($\eta = 2$). The crest propagates off-shore with speed $fd/2h_x$.

We next examine the shape of the isopycnal surfaces when $h_{xx} \neq 0$. We consider a topography such that the slope is a constant in shallow water and a much larger constant in deep water. These two regions are connected with an intermediate region, the shelf break, where h_x increases rapidly. We can see from Eq. (7c) that if $h_{xx}h/h_x^2 > 2.0$, at some point in this shelf-break region, then $p_x > 0$ at that point for all time. Therefore, with the onset of upwelling an upward bulge in the isopycnal pattern will develop and be maintained in the shelf-break region until η there exceeds 2.0. This upward bulge exists independently of that formed in shallow water when $\eta_c \geq 2$. The complex time history of the isopycnal surfaces results from a fairly simple model.

This model requires only the specification of the time history of alongshore wind and a value for d. We now address the problem of determining this parameter. If this layer were considered to have a constant eddy diffusivity A_v, Csanady (1976) has estimated that $A_v = u^{*2}/200f$. For the bottom layer, we take $u^* = u_B^*$. In the absence of other mechanisms to maintain turbulent mixing, we assume that u_B^* is generated by the geostrophic alongshore current. Meteorological data, taken by many investigators over a range of stability conditions (Monin and Yaglom, 1971), indicate that the ratio of u_B^* to the geostrophic velocity ranges between 0.01 and 0.05. We therefore take $u_B^* = 0.03v_B$. Now during the spin-up process v_B ranges from zero to V and we take $v_B = V/2$ and $u_B^* = 0.015\,V$. Since $d = (A_v/2f)^{1/2} = u_B^*/20f$ and $V = u_w^{*2}/fd$ we find that

$$u_B^* = 0.015V = 0.30u_w^{*2}/u_B^*.$$

Hence

$$u_B^* \approx u_w^*/2, \tag{10a}$$

$$d = u_w^*/40f, \tag{10b}$$

$$A_v = u_w^{*2}/800f, \tag{10c}$$

$$V = 40u_w^*, \tag{10d}$$

where $u_w^* = (|\tau|/\rho_r)^{1/2}$.

For a time-varying wind we should take u_w^* in (10b) to be some average value of $(|\tau|/\rho_r)^{1/2}$. At this point, the parameters of the model are all specified and we now estimate the magnitude of terms neglected in the analysis to determine conditions under which the model may apply.

4. Applicability of the model and baroclinic effects

In order to determine the consistency of the model and its parametric limitations, we consider the various assumptions of the model. Our first requirement was that $d \ll h$. Using (10b) for d, we find that

$$u_w^*/40fh \ll 1. \tag{11}$$

For $\tau = 0.5$ dyn cm^{-2} with $h = 50$ m and $f = 10^{-4}$ s^{-1}, the left-hand side of (11) is 0.04 so that this condition is fulfilled.

The ratio of nonlinear to time-dependent terms in the governing equations can be shown to be Vh_x/fh. Using (10c) in this ratio we find

$$40u_w^*h_x/fh \ll 1. \tag{12}$$

For $\tau = 0.5$ dyn cm^{-2}, $h_x = 2 \times 10^{-3}$, $h = 50$ m, $f = 10^{-4}$ s^{-1} the term on the left-hand side of (12) is 0.11 so that this condition is satisfied.

If horizontal mixing is parameterized by a constant horizontal eddy difficulty A_H, then mixing terms will be small compared to time-dependent terms if

$$40A_Hh_x^2/u_w^*h \ll 1. \tag{13}$$

For $A_H = 10^6$ cm^2 s^{-1} with the other parameters taking their previous values, the left-hand side of (13) is 0.05 so that mixing can safely be neglected.

For baroclinic effects to be small, $|hv_z/V| \ll 1$ or $ghp_x/\rho_r fV \ll 1$; this condition becomes

$$g\,|\rho_{0z}(z)|h_x^2/\rho_r f^2 \ll 1. \tag{14}$$

For $|g(\rho_{0z}/\rho_r)(z)| = 10^{-4}$ s^{-2} the left-hand side of (14) is 0.04, and this condition is satisfied.

Conditions (11)–(14) reflect the parameteric limitations on the model if the initial conditions are satisfied and the driving force, i.e., the wind stress, is independent of y. In practice, τ will vary with y over a distance L_y and the question arises whether this model can still be applied locally if this occurs. The model equations will apply locally if $v_y \ll u_x$. This limitation can be expressed as follows:

$$\frac{V}{L_y} \ll \frac{dV}{h}\frac{h_x}{h}$$

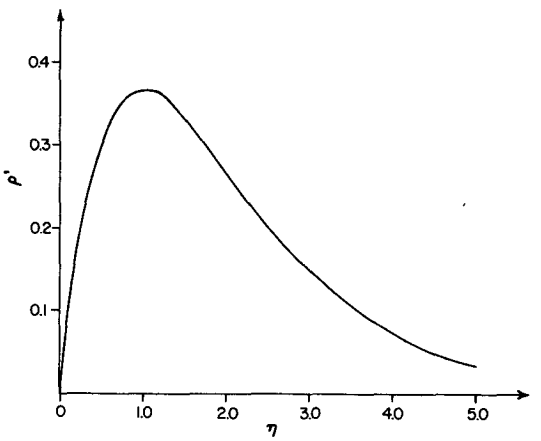

FIG. 3. The density perturbation at a point as a fuction of time for the linear bottom stress case.

or

$$L_y \gg \frac{h^2}{dh_x} = \frac{40fh^2}{u_w^* h_x}. \tag{15}$$

Using the previously specified values for f, h, u_w^*, h_x the right-hand side of (15) is 700 km. This constraint poses a strong limitation on the applicability of the theory.

The alongshore variations in wind stress which normally occur in nature will give rise directly to alongshore pressure gradients and, in transient cases, may also give rise to shelf waves. These waves will produce currents which are not tied to the local winds and our model cannot be extended to include these effects. The calculations in the Appendix of the current produced by a specified alongshore pressure gradient are valid but the very important questions relating to the source of this gradient, i.e., its generation by the spatial and temporal variations in the wind, lie beyond the scope of this work.

If the wind stress is independent of y, the errors in the theory will be due to the neglect of horizontal mixing, nonlinearities and baroclinicity.

These small corrections can be obtained using a regular perturbation approach. However, the treatment of the effects of mixing would require the assumption of an eddy diffusivity and the examination of nonlinear effects would require a knowledge of the structure of the velocity field in the boundary layers. Therefore, in this paper we will examine the effects of baroclinicity via a small perturbation analysis. This approach requires a set of dimensionless equations.

We now examine the flow of an initially linearly stratified fluid [$\rho_0(z) = \rho_r(1 - \beta z)$] over a linearly sloping bottom ($h = h_c + \alpha x$), under the linear bottom stress relation. The solution given in Eq. (7) leads us to the following choice of parameters. We let

$$\left.\begin{aligned} &V = \tau/\rho_r f d, \quad L = h_c/\alpha, \quad S = N^2\alpha^2/f^2 \\ &x' = x/L, \quad z' = z/h_c, \quad t' = t/(h_c/fd) \\ &h' = h/h_c = 1 + x', \quad u' = uh_c/Vd \\ &v' = v/V, \quad w' = wh_c/Vd\alpha \\ &p' = p/\rho_r f V L, \quad \rho' = \rho g f/\rho_r N^2 V \alpha \end{aligned}\right\}. \tag{16}$$

We now drop the primes on the dimensionless quantities. The dimensionless governing equations are as follows:

$$\int_{-h}^{0} v_t dz + v(x, -h, t) = 1, \tag{17a}$$

$$v = p_x, \tag{17b}$$

$$u = -v_t, \tag{17c}$$

$$p_z = -S\rho, \tag{17d}$$

$$u_x + w_z = 0, \tag{17e}$$

$$\rho_t = w. \tag{17f}$$

We now assume $S \ll 1$, and expand the dependent variables as

$$(u,v,w,p,\rho) = \sum_{n=0}^{\infty} S^n(u,v,w,p,\rho)_n. \tag{18}$$

Substituting Eq. (18) into (17) leads to a set of equations in increasing powers of S. The equations of order S^0 yield solutions which are the dimensionless versions of equation (7). In particular

$$v_0 = (1 - e^{-\eta}), \tag{19a}$$

$$\rho_0 = |z|\eta e^{-\eta}/h. \tag{19b}$$

The flow at order S^1 is driven by the zeroth-order horizontal density gradient. In particular,

$$\int_{-h}^{0} v_{1t} dz + v_1(x, -h, t) = 0, \tag{20a}$$

$$v_{1z} = -\rho_{0x}. \tag{20b}$$

Eq. (20b) is integrated in z; the surface velocity appears as an integration "constant." Substituting the integral of Eq. (20b) into (20a) leads to the following solution for $v_1(x,z,t)$:

$$v_1 = e^{-\eta}[(\eta + \eta^2/2 - \eta^3/3)/3 - (z^2/2h^2)(2\eta - \eta^2)]. \tag{21}$$

The baroclinic correction to the alongshore velocity is positive (negative) at the surface when η is less (greater) than 2.6. The baroclinic correction decreases (increases) as $|z|$ increases for η less (greater) than 2.0. We note that when $S\eta^3/9$ is order one, the regular perturbation approach breaks down since $Sv_1/(v_0 - 1)$ is then of order one at these very long times. However, if the wind stress is episodic in nature, this nonuniformity will not be important and (8) will be valid.

Now that the basic model and its limitations have been explored, we turn to a comparison of model predictions with a set of field observations.

5. Comparison of observations with theory

During the summer of 1976, personnel from North Carolina State University were involved in an Onslow Bay, North Carolina shelf processes study. Physical data were collected from six fixed current meter moorings in Onslow Bay (Fig. 4). Mooring locations, experiment period, instrument types and instrument depths are given in Table 1. The Aanderaa-RCM4 current meters recorded temperature, pressure and current speed and direction at 15 min intervals. These measurements had precisions

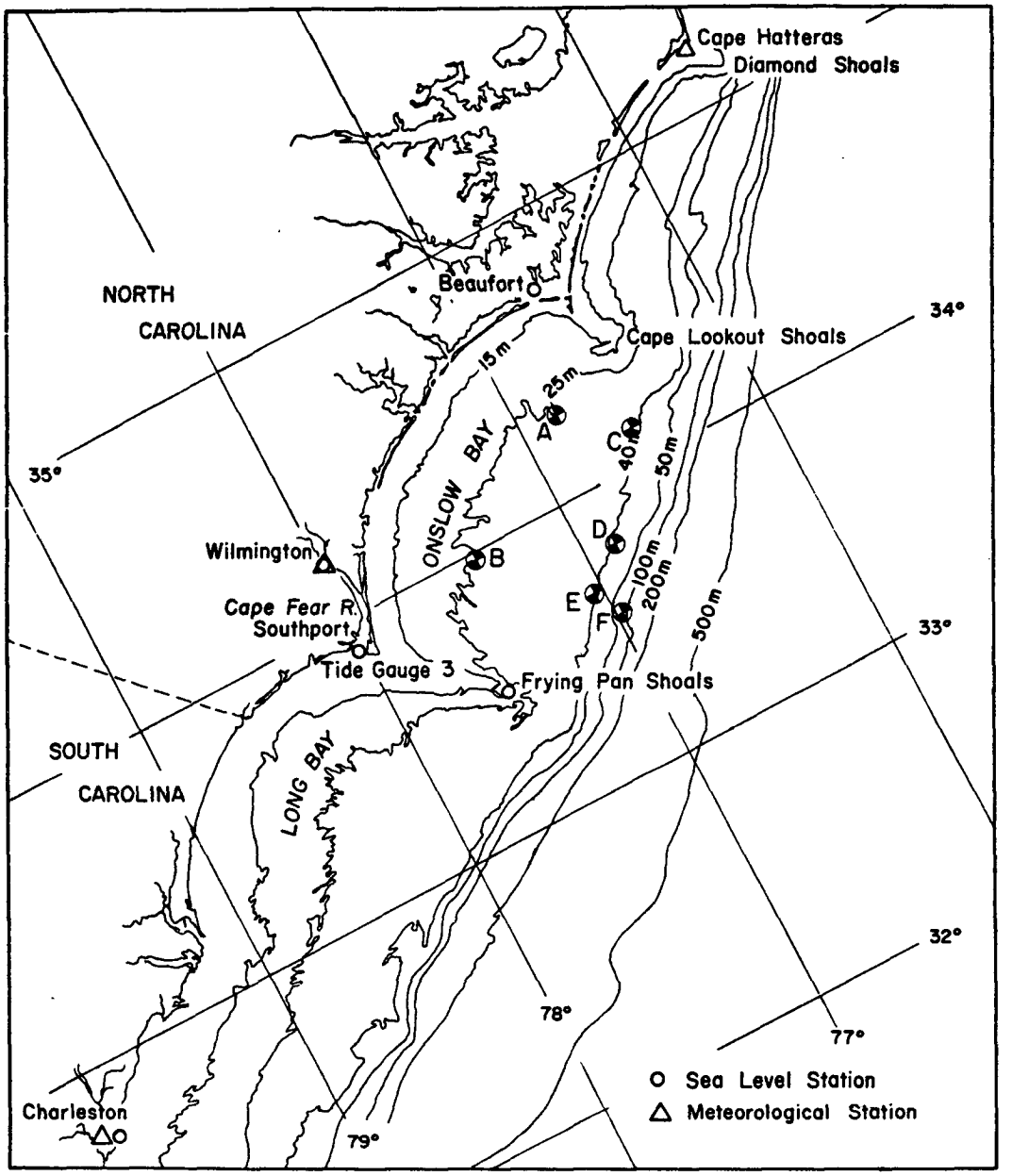

FIG. 4. Carolina Capes region, showing locations of sea level and meteorological stations and current.

of ±0.15°C, ±1%, ±1 cm s^{-1} and ±5°C, respectively. Additionally, Endeco-105 current meters, General Oceanics-2010 inclinometers and General Oceanics-2070 thermographs recorded data at 30 min intervals. Precisions associated with these instruments are, respectively, ±8 cm s^{-1}, ±5°, ±3 cm s^{-1}, ±5° and ±0.55°C.

The data were 3 h low-passed to reduce high-frequency noise due to gravity wave aliasing and other contamination and then the resulting record was 40 h low-passed to remove tidal and subtidal period bands. This record was divided into 6 h subsamples and the time series of data were reconstructed. Wind-vector and wind-stress components were computed for a rotated coordinate system, such that the y axis was qualitatively "alongshore," with the positive vector sense in the direction toward which the wind blows. Complete discussions of current and meteorological data processing can be found in Pietrafesa *et al.* (1978).

Contemporaneous hydrographic data were obtained from several cruises in Onslow Bay during the summer of 1976. These data consist of temperature, salinity and nutrient measurements which were

TABLE 1. Instrument moorings and element locations.

Mooring	Inclusive dates (1976)	Latitude Longitude	Loran A	Water depth (m)	Instrument depth (m)	Instrument type	Instrument No.
A	8 Jul	34°18'N	4855	28	12	Endeco C.M.	316
(Albatross)	25 Aug	76°50.6'W	2060		25	Inclimometer	M
B	7 Jul	33°58.2'N	4894	28	12	Endeco C.M. 247	247
(Brant)	25 Aug	77°25.8'W	2493		25	Inclimometer	2
					26	Thermograph	5
C	22 Jun	34°06.8'N	4780	40	22	Aanderaa	2254
(Cormorant)	21 Sep	76°35.6'W	2030		28.5	Thermograph	4
					35	Aanderaa	1905
D	8 Jul	33°46.7'N	4777	40	22	Aanderaa	2259
(Dunlin)	21 Sep	76°55.1'W	2325		28.5	Thermograph	7
					35	Aanderaa	1908
E	22 Jun	33°39'N	4774	40	22	Aanderaa	2256
(Elder)	21 Sep	77°03'W	2445		28.5	Thermograph	3
					35	Aanderaa	1907
F	8 Jul	33°34.6'N	4743	70	22	Aanderaa	2255
(Foster's Tern)	21 Sep	76°56'W	2432		65	Aanderaa	1906

collected using standard oceanographic techniques. Singer *et al.* (1977) give a detailed description of hydrographic methods, cruise tracks and data processing.

Moorings C, D, E and F were located in the mid to outer portion of Onslow Bay and in the area often directly influenced by the Gulf Stream, while A and B moorings are only occasionally directly influenced by the Gulf Stream.

During the period 23 June–7 August 1976, Gulf Stream meanders, wind-forced events and Gulf Stream spin-off filament and spun-up eddy events are evident both in the Onslow Bay moored meter data and in satellite Very High-Resolution Radiometer Imagery (VHRR). An event chosen for the model comparison during this time (21–26 July) is well defined by temperature, current, sea level and coastal wind data.

Coastal winds collected at Wilmington, North Carolina (Fig. 5e) indicate that from 23 June–2 August the low-frequency winds were generally from the south-southwest with only four brief intermittent reversals totaling 8 days over the 40-day period. During the period 21–26 July, the winds blew with moderate but persistent intensity from the southwest. Along the North Carolina coast southwesterly winds typically result in a drop of sea level at the coast and a set-up of sea level offshore in concert with a surface Ekman transport offshore; in a conventional sense, the observed wind field was upwelling favorable. Mean current velocity vectors associated with this wind event are shown in Figs. 5a–5c. It should be noted that the "top" meters at moorings D and E are actually 22 m from the surface and 18 m from the bottom. They are out of the surface and bottom frictional layers and therefore measure the interior flow induced by direct frictional set up of the sea surface. The drop of sea level at Charleston is of the order of 15 cm during the event. If this drop were used to project a coastal set-down and an offshore set up of the surface, then from geostrophy the interior flow at E would be the order of 20 cm s^{-1}; it was measured at 25 cm s^{-1} as shown in Fig. 5c. Directional information from E bottom (Fig. 5d) indicates flow directly onshore (northwest) rather than alongshore. Thus, it appears that two mechanisms are operating at this location: a geostrophic response in the interior and wind induced upwelling near the bottom. This same scenario is observed at mooring D. An alongshore geostrophic current is seen at D-top (Fig. 5b), while D-bottom (Fig. 5a) indicates flow directly onshore. It is of note that during the entire event period, the Gulf Stream Front was well offshore of the shelf break.

Onshore and upward transport of cold slope waters during this period is indicated by drops in temperature at the upper and lower sensors at mooring sites B, D, E and F as noted (Figs. 6a–6f). This decrease persists as a distinct feature at all sites for several days.

Comparison of the temperature records from the bottom sensors at moorings F, E, D and B, in order (Figs. 6a, 6c, 6e and 6f), shows that not only were isotherms elevated at the onset of the event, but that cold water spilled across the shelf in a bottom layer at least 5 m thick. These data also suggest that the cold water moved onshore, upward and clockwise along the bottom. Given the positions of the moorings and the time the cold water arrived at each, it appears that the bottom intrusion entered in the

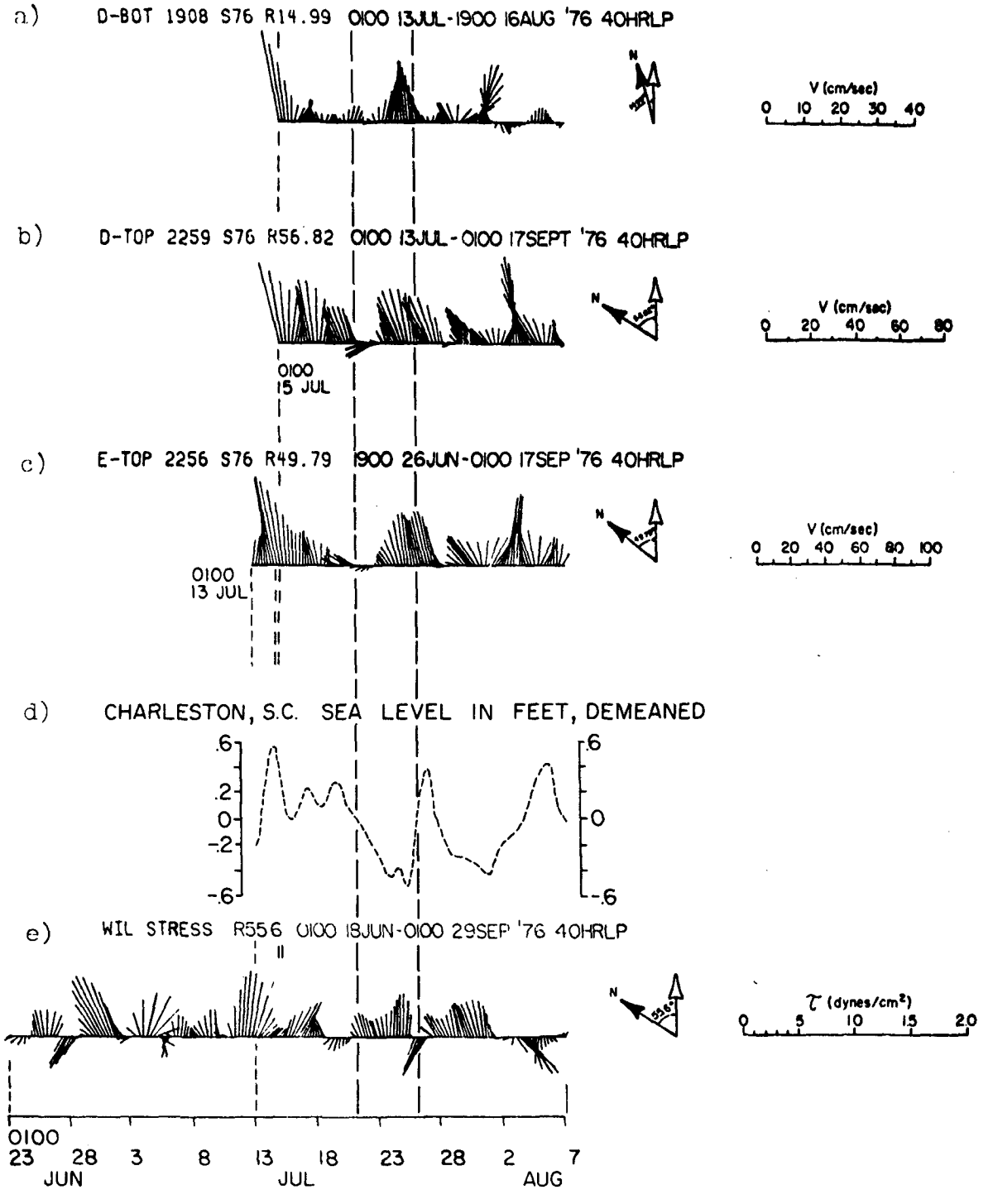

FIG. 5. (a) 40HRLP current sticks from meter D-bottom, (b) 40HRLP current sticks from meter D-top, (c) 40HRLP current sticks from meter E-top, (d) 40HRLP sea level from Charleston, (e) 40HRLP wind-stress stocks from Wilmington.

southern portion of Onslow Bay (sites F, E, D), moved onshore (site B) crossing bottom contours.

In the region under consideration, $f = 0.8 \times 10^{-4}$ s^{-1} and the mean alongshore wind stress during the upwelling period 21–26 July is 0.23 dyn cm^{-2}. This yields a frictional velocity $u_w^* = 0.48$ cm s^{-1}. Using Eqs. (10b)–(10d), we find that $A_v = 3.6$ cm^2 s^{-1}, $d = 1.47$ m and $V = 19$ cm s^{-1}. The density disturbance at any location reaches a maximum when η $(=fdt/h) = 1.0$, where t is the elapsed time from

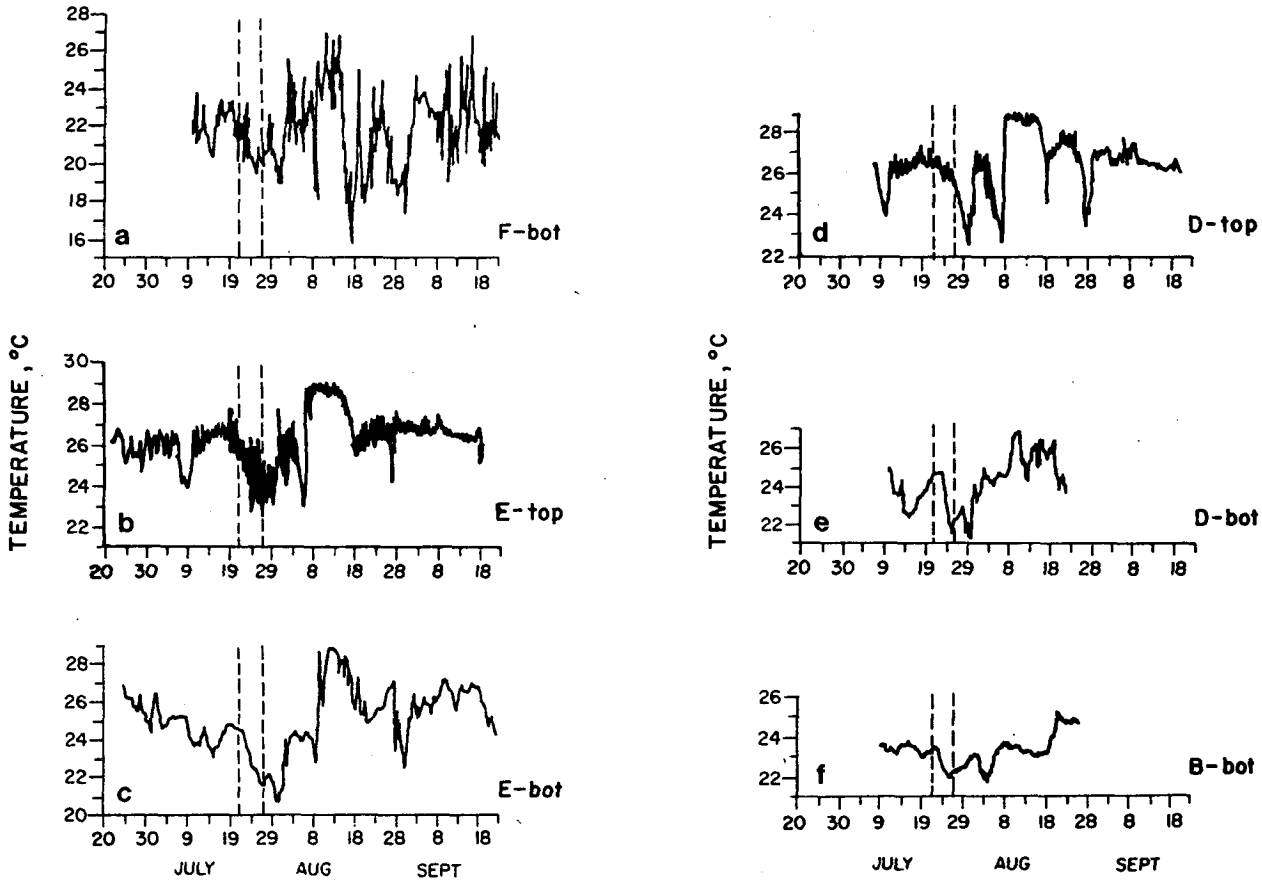

FIG. 6. (a) 3HRLP temperature from meter F-bottom, (b) 3HRLP temperature from meter E-top, (c) 3HRLP temperature from meter E-bottom, (d) 3HRLP temperature from meter D-top, (e) 3HRLP temperature from meter D-bottom, (f) 3HRLP temperature from meter B-bottom.

the onset of upwelling favorable winds. When the depth is 28 m (site B), $\eta = 1$ when $t = 66$ h. When the depth is 40 m (site E), $\eta = 1$ when $t = 95$ h. The data, (Figs. 6f and 6c) indicate that the temperature bottoms are at 60 and 96 h at sites B and E, respectively, in fair agreement with the predicted times. The maximum observed velocities at sites D and E (Figs. 5b and 5c) are 25 cm s^{-1} as opposed to the predicted value of 19 cm s^{-1}. The Gulf Stream, which is some 20 km east of the mooring locations may account for this discrepancy by tending to augment the northeasterly flow.

This tentative comparison with data indicates that the simple model developed in this paper may have some validity although further comparisons should be undertaken.

6. Conclusions

We have considered a dynamically simple model which describes the time-dependent upwelling process over the outer shelf and slope regions. The dynamics described by this model are as follows.

With the onset of upwelling favorable winds an onshore water column flow is set up to balance the offshore top layer transport. The Coriolis force due to this onshore flow generates an alongshore velocity and its associated boundary layer. The bottom layer carries mass into shallow water which causes a decrease in the onshore water column velocity. This spin-up process occurs most rapidly in shallow water which leads to an alongshore jet with negative vorticity.

The vertical velocity is first positive due to the kinematic effect of onshore flow into shallow water; at later times the vertical velocity becomes negative as downward suction into the lower layer overcomes the kinematic effect. The density disturbance first increases then decreases reflecting the change in sign of the vertical velocity.

The variation in spin-up time across the shelf is reflected in the time history of the shape of the isopycnal surfaces. Away from the shelf break and for early times these surfaces slope upward in the onshore direction. Later, an upward bulge in the isopycnal surfaces forms at the coast and propagates seaward. Additionally, if the shelf break is sharp enough, i.e., $h_{xx}h/h_x^2 > 2$, a second upward bulge

in the isopycnal surfaces develops there at the onset of upwelling favorable winds and is present throughout most of the upwelling process.

The predictions of the model were compared with a set of field observations. Additional verification is called for.

Acknowledgments. The authors gratefully acknowledge the support for this study by the Department of Energy under Contract DOE AS09-76-EY00902. Portions of the description of the observations appeared in Hoffman (1979).

APPENDIX

The Effect of an Alongshore Pressure Gradient

As discussed in Section 3, if a time-dependent alongshore pressure gradient, independent of x, y and z, is imposed on the fluid, the velocity field due to the wind stress will be modified. For the case of the linear bottom stress, wind stress and pressure gradient driven flows can be summed and we neglect here the previously calculated wind-stress effect.

In the presence of a time-dependent alongshore pressure gradient, Eqs. (1) and (4b) become, for the linear bottom stress case,

$$hv_t + fdv = -hp_y(t)/\rho_r, \tag{A1}$$

$$u = -v_t/f - p_y(t)/\rho_r f. \tag{A2}$$

Eq. (A1) can be integrated to find $v(x,t)$. This result is used in equation (A2) to find $u(x,t)$. The solutions are

$$\rho_r v = -\int_0^t p_y(t') \exp[-fd(t - t')/h]dt', \tag{A3}$$

$$u = dv/h. \tag{A4}$$

Eq. (A4) reflects the constraint, under the rigid-lid approximation, that the interior offshore volume flux hu must be balanced by the onshore bottom flux dv.

We now consider two special cases for $p_y(t)$. First, let $p_y(t)/\rho_r = GU(t)$, where G is a constant and $U(t)$ is the Heaviside stepfunction. Eq. (A3) then yields the solution

$$v = -(Gh/fd)(1 - e^{-\eta}),$$

where $\eta = fdt/h$. For small η, $v = -Gt$, while for large η, $v = -Gh/fd$. We can show, for all t, that $v_x \geq 0$ so that the maximum alongshore speed is in deep water.

We finally consider $p_y/\rho_r = G \sin(\omega t)$. Eq. (A3) yields the solution

$$v = -(G/w)\chi(1 + \chi^2)^{-1/2}[\sin[\omega t - \tan^{-1}(\chi)] + \sin[\tan^{-1}(\chi)]e^{-\eta}],$$

where $\chi = \omega h/fd$, $\eta = fdt/h$. We note that after the transient term, $e^{-\eta}$, decays, v lags the driving force, $-G \sin(\omega t)$, by $\tan^{-1}(\chi)$ which increases seaward, and the magnitude of the maximum velocity also increases seaward. We must require that $\omega \ll f$ for the quasi-geostrophic analysis to apply ($|u_+| \ll fv$), and that $h/d \gg 1$. Therefore, χ, which is proportional to the ratio of decay time to the period of oscillation, may be either large or small. If $\chi \gg 1$,

$$v = -(G/\omega)[e^{-\eta} - \cos(\omega t)],$$

and the horizontal shear is due only to the transient term. In this case $\omega t/\eta \gg 1$ and several periods of oscillation may occur before the transient term decays. In deep water, where $\eta \ll 1$, the velocity will vary from $-2G/\omega$ to $+G\eta/\omega$. In shallow water, where η may be large, v will vary from $-G/\omega$ to $+G/\omega$. The velocity may be positive in shallow water and at the same time be negative in deep water; this would give rise to countercurrents.

REFERENCES

Allen, J. S., 1980: Models of wind-driven currents on the continental shelf. *Annual Reviews Of Fluid Mechanics*, M. Van Dyke, J. V. Wehausen and J. L. Lumley, Eds., Vol. 12, Annual Reviews, Inc., 389–433.

Blanton, J. O., and L. J. Pietrafesa, 1978: Flushing of the Continental Shelf South of Cape Hatteras by the Gulf Stream. *Geophys. Res. Lett.*, **5**, 495–498.

Csanady, G. T., 1976: Mean circulation in shallow seas. *J. Geophys. Res.*, **81**, 5389–5399.

——, 1977: The coastal jet conceptual model in the dynamics of shallow seas. *The Sea*, Vol. 6, E. D. Goldberg, I. M. McCane, J. J. O'Brien and J. H. Steele, Eds., Wiley-Interscience, 117–144.

Garvine, R. W., 1971: A simple model of coastal upwelling dynamics. *J. Phys. Oceanogr.*, **1**, 169–179.

Hoffman, E., 1979: Analysis and modeling of a bottom intrusion. Dept. Marine Science and Engineering, North Carolina State University, 105 pp.

Hsueh, Y., and H. W. Ou, 1975: On the possibilities of coastal, mid-shelf, and shelf break upwelling. *J. Phys. Oceanogr.*, **5**, 670–682.

Lill, C. C., 1979: Upwelling over the shelf break. *J. Phys. Oceanogr.*, **9**, 1044–1047.

Monin, A. S., and A. M. Yaglom, 1971: *Statistical Fluid Mechanics of Turbulence*, Vol. 1. The MIT Press, 769 pp.

O'Brien, J. J., 1975: Models of coastal upwelling. *Numerical Models of Ocean Circulation*, Nat. Acad. Sci., 204–215.

Pietrafesa, L. J., 1979: On continental margin processes in the South Atlantic bight. *Trans. Amer. Geophys. Union*, **60**, 281.

——, and G. S. Janowitz, 1980: Lack of evidence of southerly propagating continental shelf waves in Onslow Bay, N.C. *Geophys. Res. Lett.*, **7**, 113–116.

——, R. D'Amato, C. D. Gabriel, R. J. Sawyer and D. A. Brooks, 1978: Onslow Bay Physical/Dynamical Experiments, Summer 1976. Center for Marine and Coastal Studies, Tech. Rep. No. 78-3, Vols. I and II.

Singer, J. J., L. P. Atkinson, W. S. Chandler and P. G. O'Malley, 1977: Hydrographic observations in Onslow Bay, North Carolina, July–August 1976 (OBIS V), Data Graphics. Georgia Marine Science Center, Tech. Rep. 77-6, 98 pp.